Hindawi Publishing Corporation
Mathematical Problems in Engineering
Volume 2010, Article ID 986319, 15 pages
doi:10.1155/2010/986319

Research Article

Periodic and Chaotic Motions of a Two-Bar Linkage with OPCL Controller

Qingkai Han,[1] Xueyan Zhao,[1] Xiaoguang Yang,[2] and Bangchun Wen[1]

[1] *School of Mechanical Engineering and Automation, Northeastern University, Shenyang 110004, China*
[2] *School of Mechanical Engineering, University of Birmingham, Birmingham B15 2TT, UK*

Correspondence should be addressed to Qingkai Han, qhan@mail.neu.edu.cn

Received 16 December 2009; Accepted 25 June 2010

Academic Editor: Irina N. Trendafilova

A two-bar linkage, which is described in differential dynamical equations, can perform nonlinear behaviors due to system parameters or external input. As a basic component of robot system, the investigation of its behavior can improve robot performance, control strategy, and system parameters. An open-plus-close-loop (OPCL) control method therefore is developed and applied to reveal and classify the complicated behaviors of a two-bar linkage. In this paper, the conception and stability of OPCL are addressed firstly. Then it is applied to the dynamical equations of two-bar linkage. Different motions including single-periodic, multiple-periodic, quasiperiodic, and chaotic motions are unfolded by numerical simulations when changing the controller parameters. Furthermore, the obtained chaotic motions are sorted out for qualitative and quantificational study using Lyapunov exponents and hypothetic possibilities of surrogate data method.

1. Introduction

A two-bar linkage, as a basic component of mechanical system, can perform nonlinear motions, among which chaotic motion is the most typically complicated one. It is known that the performance of such a mechanism is influenced by system parameters such as mass and friction coefficient, the initial states, and external input such as driving torque controlled by specially designed controller. Conversely, study on these motions can provide a novel way to improve system's performance, optimize structure design, and develop new control strategy.

For a two-bar linkage, the motions of its two rotating links can be single periodic, multiple periodic, quasiperiodic, and chaotic. In the past decades, many control strategies were explored to obtain certain motions of a two-bar linkage mechanism. A neural controller was employed to achieve two typical synchronous motions, that is, giant rotating motion and

small swing motion as stated in [1, 2]. A PD feedback controller to obtain chaotic motions for a two-bar linkage was reported in [3, 4]. The bifurcation characteristics of motions of a two-bar linkage were presented in [5]. The transferring process of a two-bar linkage from period-doubling bifurcation to chaotic motions was studied by changing control variables in [6]. In recent research, it is known that the open-plus-close-loop (OPCL) control strategy is powerful for complicated dynamic systems, as stated in [7, 8], which has been used for chaotic control of chaotic systems [9] and synchronous systems [10, 11]. Besides, the parametric OPCL method [12] and the nonlinear OPCL method were also applied for motion control of some dynamic systems [13].

In this paper, an OPCL controller is proposed for a two-bar linkage to achieve different motions as stated above. The dynamics of the two-bar linkage is modeled with nonlinear differential equations, followed by the Lyapunov stability analysis of the controlled system. By changing the two coefficient matrices **A** and **B** of the OPCL controller, we obtain typical motions of the two-bar linkage in numerical simulations including single-periodic, multiple-periodic, quasiperiodic, as well as chaotic motions. These different motions are described in both qualitative and quantificational ways, such as phase-space portraits, frequency spectra, Lyapunov exponents, and the hypothetic possibilities of surrogate data.

2. Dynamical Equations of a Two-Bar Linkage with OPCL Controller

2.1. A Dynamical System with an OPCL Controller

Let a typical dynamical system be as follows:

$$\ddot{\boldsymbol{\theta}} = \mathbf{F}(\boldsymbol{\theta}, \dot{\boldsymbol{\theta}}, t), \tag{2.1}$$

where $\theta = \{\theta_1, \theta_2, \ldots, \theta_n\}^T$ is the state variable, and n is the number of DOF of the system.

The given motion goal of the system is

$$\mathbf{g} = \{g_1, g_2, \ldots, g_n\}^T. \tag{2.2}$$

Define a tracking error of the two-bar linkage as

$$\mathbf{e} = \boldsymbol{\theta} - \mathbf{g} = \{\theta_1 - g_1, \theta_2 - g_2, \ldots, \theta_n - g_n\}^T = \{e_1, e_2, \ldots, e_n\}^T. \tag{2.3}$$

Equation (2.1) is linearized and expanded in the neighborhood of the goal via Taylor series and it becomes

$$\begin{aligned}\ddot{\boldsymbol{\theta}} = \mathbf{F}(\boldsymbol{\theta}, \dot{\boldsymbol{\theta}}, t) &= \mathbf{F}(\mathbf{g}+\mathbf{e}, \dot{\mathbf{g}}+\dot{\mathbf{e}}, t) = \mathbf{F}(\mathbf{g}, \dot{\mathbf{g}}, t) + \left(\frac{\partial \mathbf{F}(\mathbf{g}, \dot{\mathbf{g}}, t)}{\partial \mathbf{g}}\right)\mathbf{e} + \left(\frac{\partial \mathbf{F}(\mathbf{g}, \dot{\mathbf{g}}, t)}{\partial \dot{\mathbf{g}}}\right)\dot{\mathbf{e}} + \mathbf{o}^2(\mathbf{g}, \dot{\mathbf{g}}) \\ &= \mathbf{F}(\mathbf{g}, \dot{\mathbf{g}}, t) + \mathbf{J}_{\mathbf{g}}\mathbf{e} + \mathbf{J}_{\dot{\mathbf{g}}}\dot{\mathbf{e}} + \mathbf{o}^2(\mathbf{g}, \dot{\mathbf{g}}),\end{aligned} \tag{2.4}$$

where $\mathbf{J}_{\mathbf{g}}$ and $\mathbf{J}_{\dot{\mathbf{g}}}$ are Jacobian matrices of $\mathbf{F}(\mathbf{g}, \dot{\mathbf{g}}, t)$ with respect to $\mathbf{g}$ and $\dot{\mathbf{g}}$, respectively.

An OPCL controller for the system is designed as [8]

$$\mathbf{U} = \ddot{\mathbf{g}} - \mathbf{F}(\mathbf{g}, \dot{\mathbf{g}}, t) - \mathbf{J}_{\mathbf{g}}\mathbf{e} - \mathbf{J}_{\dot{\mathbf{g}}}\dot{\mathbf{e}} + \mathbf{A}\dot{\mathbf{e}} + \mathbf{B}\mathbf{e}, \tag{2.5}$$

where the term of $\ddot{\mathbf{g}} - \mathbf{F}(\mathbf{g}, \dot{\mathbf{g}}, t)$ is the open-loop part, and the term of $-\mathbf{J}_{\mathbf{g}}\mathbf{e} - \mathbf{J}_{\dot{\mathbf{g}}}\dot{\mathbf{e}} + \mathbf{A}\dot{\mathbf{e}} + \mathbf{B}\mathbf{e}$ is the closed-loop part. In this controller, the coefficient matrices $\mathbf{A}$ and $\mathbf{B}$ are assumed to be diagonal.

The controlled system, that is, the dynamical system with its OPCL controller, is rewritten as follows:

$$\begin{aligned}\ddot{\boldsymbol{\theta}} &= \mathbf{F}(\boldsymbol{\theta}, \dot{\boldsymbol{\theta}}, t) + \mathbf{U} \\ &= \mathbf{F}(\mathbf{g}, \dot{\mathbf{g}}, t) + \mathbf{J}_{\mathbf{g}}\mathbf{e} + \mathbf{J}_{\dot{\mathbf{g}}}\dot{\mathbf{e}} + \mathbf{o}^2(\mathbf{g}, \dot{\mathbf{g}}) + \ddot{\mathbf{g}} - \mathbf{F}(\mathbf{g}, \dot{\mathbf{g}}, t) - \mathbf{J}_{\mathbf{g}}\mathbf{e} - \mathbf{J}_{\dot{\mathbf{g}}}\dot{\mathbf{e}} + \mathbf{A}\dot{\mathbf{e}} + \mathbf{B}\mathbf{e} \\ &= \ddot{\mathbf{g}} + \mathbf{A}\dot{\mathbf{e}} + \mathbf{B}\mathbf{e} + \mathbf{o}^2(\mathbf{g}, \dot{\mathbf{g}}).\end{aligned} \tag{2.6}$$

The tracking error equation defined as (2.3) can be deduced as follows with omitting higher-order term:

$$\ddot{\mathbf{e}} = \ddot{\boldsymbol{\theta}} - \ddot{\mathbf{g}} = \ddot{\mathbf{g}} + \mathbf{A}\dot{\mathbf{e}} + \mathbf{B}\mathbf{e} + \mathbf{o}^2(\mathbf{g}, \dot{\mathbf{g}}) - \ddot{\mathbf{g}} = \mathbf{A}\dot{\mathbf{e}} + \mathbf{B}\mathbf{e}. \tag{2.7}$$

It is noticed that, if the controlled system of (2.6) is asymptotically stable when coefficient matrices $\mathbf{A}$ and $\mathbf{B}$ are constant and with negative real parts of eigenvalues, that is, their elements a_{ii} and b_{ii} should be negative, (2.7) can be rewritten in an expanded form as

$$\begin{Bmatrix} \ddot{e}_1 \\ \ddot{e}_2 \\ \vdots \\ \ddot{e}_n \end{Bmatrix} = \operatorname{diag}(a_{11}, a_{22}, \ldots, a_{nn}) \begin{Bmatrix} \dot{e}_1 \\ \dot{e}_2 \\ \vdots \\ \dot{e}_n \end{Bmatrix} + \operatorname{diag}(b_{11}, b_{22}, \ldots, b_{nn}) \begin{Bmatrix} e_1 \\ e_2 \\ \vdots \\ e_n \end{Bmatrix} = \begin{Bmatrix} a_{11}\dot{e}_1 + b_{11}e_1 \\ a_{22}\dot{e}_2 + b_{22}e_2 \\ \vdots \\ a_{nn}\dot{e}_n + b_{nn}e_n \end{Bmatrix}. \tag{2.8}$$

Thus, if $\ddot{e}_i = a_{ii}\dot{e}_i + b_{ii}e_i$ $(i = 1, 2, \ldots, n)$ is asymptotically stable, the system is also stable. Therefore, the aforementioned assumption is true.

A Lyapunov function V is defined as

$$V(\dot{e}_i, e_i) = \frac{b_{ii}}{2a_{ii}}e_i^2 - \frac{1}{2a_{ii}}\dot{e}_i^2 > 0. \tag{2.9}$$

Then

$$\dot{V}(\dot{e}_i, e_i) = \frac{b_{ii}e_i\dot{e}_i - \dot{e}_i\ddot{e}_i}{a_{ii}} = \frac{b_{ii}e_i\dot{e}_i - \dot{e}_i(a_{ii}\dot{e}_i + b_{ii}e_i)}{a_{ii}} = -\dot{e}_i^2 < 0. \tag{2.10}$$

According to the Lyapunov stability theory, it is proved that the error equation of (2.7) is asymptotically stable if the real parts of the eigenvalues of the coefficient matrices **A** and **B** are negative. It can be found that such an OPCL controller is reliable enough to be applied on a two-bar linkage in order to get different motions as expected and these motions are asymptotically stable.

2.2. Dynamic Equations of Two-Bar Linkage

A two-bar linkage is shown in Figure 1. Its two joints can be driven, respectively, at o_1 and o_2, so that the upper link (Link 1) and the lower link (Link 2) can rotate, respectively, around their own joints of o_1 and o_2 within the range of $[-\pi,\pi]$. The upper joint o_1 is fixed on the ground.

In coordinate system O_1xy, as shown in Figure 1, θ_1 is the rotating angle of Link 1 with respect to y-axis, and θ_2 is the rotating angle of Link 2 with respect to the centerline of Link 1. The dynamical equations of the two-bar linkage are given as follows:

$$\begin{bmatrix} M_{11} & M_{12} \\ M_{21} & M_{22} \end{bmatrix} \begin{Bmatrix} \ddot{\theta}_1 \\ \ddot{\theta}_2 \end{Bmatrix} + \begin{Bmatrix} C_1(\theta_1, \theta_2, \dot{\theta}_1, \dot{\theta}_2) \\ C_2(\theta_1, \theta_2, \dot{\theta}_1, \dot{\theta}_2) \end{Bmatrix} + \begin{Bmatrix} K_1(\theta_1, \theta_2) \\ K_2(\theta_1, \theta_2) \end{Bmatrix} = \begin{Bmatrix} \tau_1 \\ \tau_2 \end{Bmatrix}, \tag{2.11}$$

where

$$\begin{aligned} M_{11} &= m_1 d_1^2 + m_2\left(l_1^2 + d_2^2 + 2l_1 d_2 \cos\theta_2\right) + I_1 + I_2, \\ M_{21} &= m_2\left(d_2^2 + l_1 d_2 \cos\theta_2\right) + I_2, \\ M_{12} &= m_2\left(d_2^2 + l_1 d_2 \cos\theta_2\right) + I_2, \\ M_{22} &= m_2 d_2^2 + I_2, \\ C_1(\theta_1, \theta_2, \dot{\theta}_1, \dot{\theta}_2) &= -m_2 l_1 d_2 \dot{\theta}_2^2 \sin\theta_2 - 2m_2 l_1 d_2 \dot{\theta}_1 \dot{\theta}_2 \sin\theta_2, \\ C_2(\theta_1, \theta_2, \dot{\theta}_1, \dot{\theta}_2) &= m_2 l_1 d_2 \dot{\theta}_1^2 \sin\theta_2, \\ K_1(\theta_1, \theta_2) &= (m_1 d_1 + m_2 l_1) g \sin\theta_1 + m_2 d_2 g \sin(\theta_1 + \theta_2), \\ K_2(\theta_1, \theta_2) &= m_2 g d_2 \sin(\theta_1 + \theta_2). \end{aligned} \tag{2.12}$$

In (2.11), m_i is the mass of Link i, $i = 1,2$; I_i is the moment of inertia of Link i with respect to its mass center, $i = 1,2$; d_i is the distance between Link i and joint i, $i = 1,2$; g is the acceleration of gravity; τ_i is driving moment in joint i, $i = 1,2$.

Equation (2.11) can be rewritten in the following form, which is also in the form of (2.1):

$$\begin{Bmatrix} \ddot{\theta}_1 \\ \ddot{\theta}_2 \end{Bmatrix} = \begin{bmatrix} H_{11} & H_{12} \\ H_{21} & H_{22} \end{bmatrix} \begin{Bmatrix} R_1 \\ R_2 \end{Bmatrix}, \tag{2.13}$$

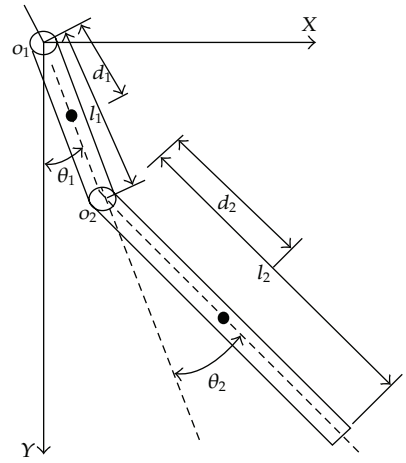

Figure 1: The schematic diagram of a two-bar linkage.

Table 1: The values of structural parameters of the two-bar linkage.

Parameter	m_1	m_2	I_1	I_2	l_{c1}	l_{c2}	l_1	l_2	g
Value	1	1	0.083	0.33	0.5	1	1	2	9.8

where

$$\begin{bmatrix} H_{11} & H_{12} \\ H_{21} & H_{22} \end{bmatrix} = \begin{bmatrix} M_{11} & M_{12} \\ M_{21} & M_{22} \end{bmatrix}^{-1}, \qquad \begin{Bmatrix} R_1 \\ R_2 \end{Bmatrix} = \begin{Bmatrix} \tau_1 - C_1(\theta_1, \theta_2, \dot{\theta}_1, \dot{\theta}_2) - K_1(\theta_1, \theta_2) \\ \tau_2 - C_2(\theta_1, \theta_2, \dot{\theta}_1, \dot{\theta}_2) - K_2(\theta_1, \theta_2) \end{Bmatrix}. \tag{2.14}$$

3. Simulations on Different Motions of Two-Bar Linkage

3.1. Conditions and Simulation Steps

In numerical simulations, the dimensionless structural parameters of the two-bar linkage are used and listed in Table 1.

The goal trajectories of the two rotating angles of the two links, θ_1 and θ_2, are designed as

$$\theta_1(t) = \sin(t), \qquad \theta_2(t) = \sin(t). \tag{3.1}$$

The simulation steps, mainly referring to the system of (2.6), are listed herein.

(1) Set the initial states and the structural parameter values of the two-bar linkage and the total number of simulation n.

(2) Set the control parameter matrices **A** and **B** of the OPCL controller of (2.5).

(3) Set the goal trajectory of (3.1).

(4) Calculate the joint angles based on (2.6) using the fourth-order Runge-Kutta method.

Table 2: The values of control parameters for different motions.

Control parameter **A**	Control parameter **B**	Motion patterns	Simulation results
A = diag(−10, −10)	**B** = diag(−20, −20)	Single-periodic motions	Section 3.2
A = diag(−16, −16)	**B** = diag(−3, −9)	Multiple-periodic motions	Section 3.3
A = diag(−8, −8)	**B** = diag(−4, −8)	Quasiperiodic motions	Section 3.4
A = diag(−2.5, −2.5)	**B** = diag(−7, −7)	Chaotic motions	Section 3.5

With different values of **A** and **B** of the OPCL controller, the two-bar linkage can achieve different motions including single-periodic, multiple-periodic, quasiperiodic, and chaotic motions. The typical parameter values of **A** and **B** and their corresponding motions are listed in Table 2. They are illustrated in the following sections, which are also listed in the fourth column of Table 2.

The obtained motions of link joints can be investigated qualitatively and quantificationally in different ways, including observation of frequency spectra and estimation of nonlinear parameters. Single- or multiamplitude lines in frequency spectra indicate a periodic motion or a multiple-periodic motion. Wide-range frequency distributions are often generated from quasiperiodic motion and chaotic motion. In Poincare mapping plots, one single point or some scattered points are often mapped by periodic motions whereas attractors with concentrated area and so-called strange attractors are mostly from either quasiperiodic or chaotic motions. In addition, for chaotic motions, there are also some critical methods to judge, for example, the well-known nonlinear parameter estimation of positive maximum Lyapunov exponent [14, 15] and the checking possibility of surrogate data method [16] which is powerful to distinguish a chaotic motion from a random one.

3.2. *Single-Periodic Motions*

Given **A** = diag(−10, −10) and **B** = diag(−20, −20), the two-bar linkage can achieve single-periodic motions. The simulated motions with initial conditions of $\theta_1 = 1$, $\dot{\theta}_1 = 0$, $\theta_2 = 1$, and $\dot{\theta}_2 = 0$ are shown in Figure 2.

In Figures 2(a) and 2(b), the motions of θ_1 and θ_2 are obviously periodic, that is, harmonic. The two phase plane portraits of θ_1 and θ_2, shown in Figures 2(c) and 2(d), are closed curves, which prove that the motions of the two-bar linkage are stable. Furthermore, the Poincare mapping portrait of each has only one isolated point, as shown in Figures 2(e) or 2(f). The frequency spectra of the two rotating angles show that there exists only single dominant frequency of about 0.16 Hz, as shown in Figures 2(g) and 2(h). The simulations can also show that periodic motions of the two-bar linkage are stable in this case.

3.3. *Multiple-Periodic Motions*

Given **A** = diag(−16, −16) and **B** = diag(−3, −9), the two-bar linkage can realize multiple-periodic motions. The typical simulated motions of the two rotating angles are shown in Figure 3 with initial conditions of $\theta_1 = 1$, $\dot{\theta}_1 = 0$, $\theta_2 = 1$, and $\dot{\theta}_2 = 0$.

In Figures 3(a) and 3(b), the motions of θ_1 and θ_2 are also periodical but with other harmonic components. The two phase plane portraits of θ_1 and θ_2, shown in Figures 3(c) and 3(d), are closed curves, which can indicate that the motions of the two-bar linkage are stable. Accordingly, the Poincare mapping portrait of each, shown in Figure 3(e) or 3(f), has some

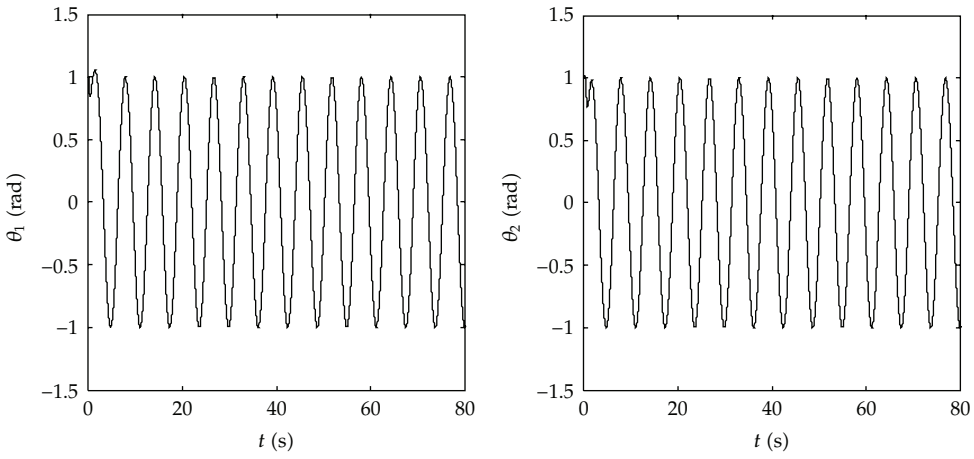

(a) Time history of θ_1

(b) Time history of θ_2

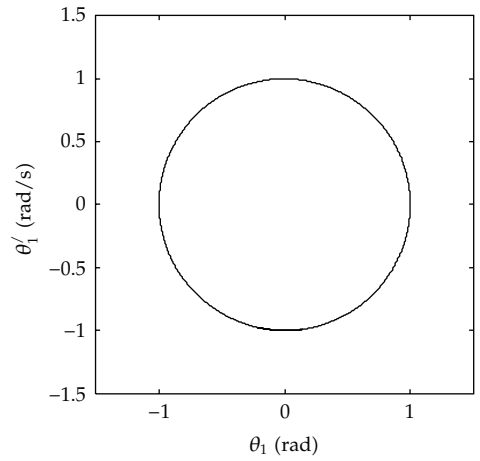

(c) Phase-plane portrait of θ_1

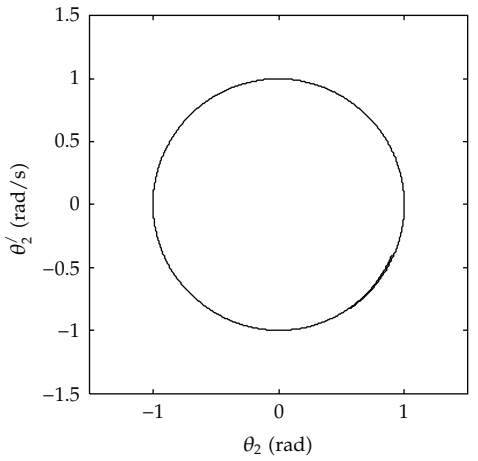

(d) Phase-plane portrait of θ_2

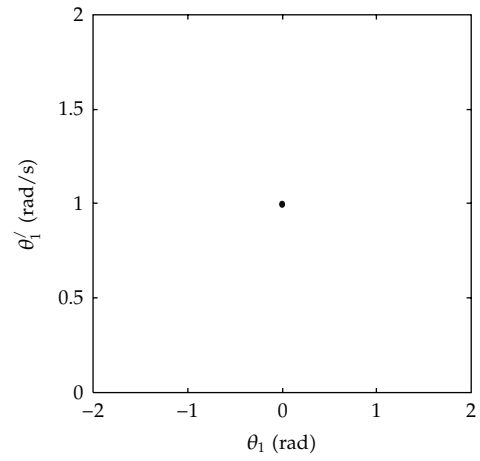

(e) Poincare mapping of θ_1

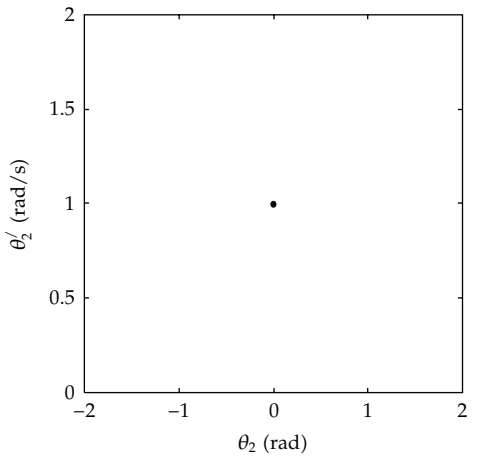

(f) Poincare mapping of θ_2

Figure 2: Continued.

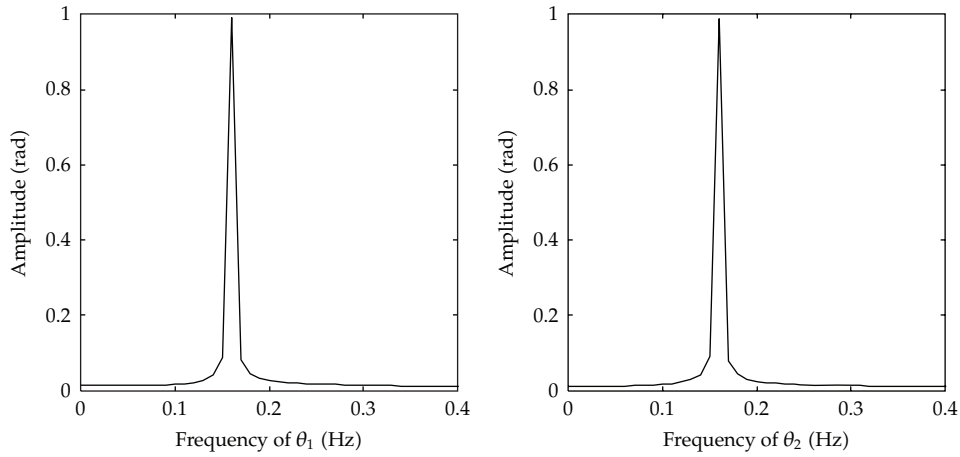

(g) Amplitude spectrum of θ_1 (h) Amplitude spectrum of θ_2

Figure 2: Single-periodic motions.

isolated points. There also exist more than two and four obvious frequency lines, as shown in Figures 3(g) and 3(h), which show that the multiperiodic motions of the two-bar linkage are stable in this case.

3.4. Quasiperiodic Motions

Given $\mathbf{A} = \text{diag}(-16, -16)$ and $\mathbf{B} = \text{diag}(-3, -9)$, the two-bar linkage can realize quasiperiodic motions. The simulated motions of the two joints are shown in Figure 4 with the initial conditions of $\theta_1 = 1$, $\dot{\theta}_1 = 0$, $\theta_2 = 1$, and $\dot{\theta}_2 = 0$.

It can be seen from Figure 4 that the motions of θ_1 and θ_2 are complex. Both the time histories and the phase plane portraits of θ_1 and θ_2 are difficult to distinguish the motion type rather than traditional harmonics. The Poincare mapping portrait of each, shown in Figures 4(e) and 4(f), is the concentrated stick-like area. More than six and eight frequency lines appear in the corresponding frequency spectra of θ_1 and θ_2 shown in Figures 4(g) and 4(h). The simulations can also show that the motions of the two-bar linkage are quasiperiodic in this case.

3.5. Chaotic Motions

Given $\mathbf{A} = \text{diag}(-2.5, -2.5)$ and $\mathbf{B} = \text{diag}(-7, -7)$, the two-bar linkage can realize chaos motions. The simulated chaotic motions are shown in Figure 5, in the case of the initial conditions of $\theta_1 = 1$, $\dot{\theta}_1 = 0$, $\theta_2 = 1$, and $\dot{\theta}_2 = 0$.

From Figures 5(a) and 5(b), the simulated responses of θ_1 and θ_2 are irregular without obvious periods. The two phase plane portraits (shown in Figures 5(c) and 5(d)) and the Poincare mapping (shown in Figures 5(e) and 5(f)) of θ_1 and θ_2 illustrate irregular shape or strange attractors. Their corresponding amplitude spectra also unfold multifrequency lines and explicit broadband ranges. According to the qualitative theory of chaos, these motions are chaotic in this case.

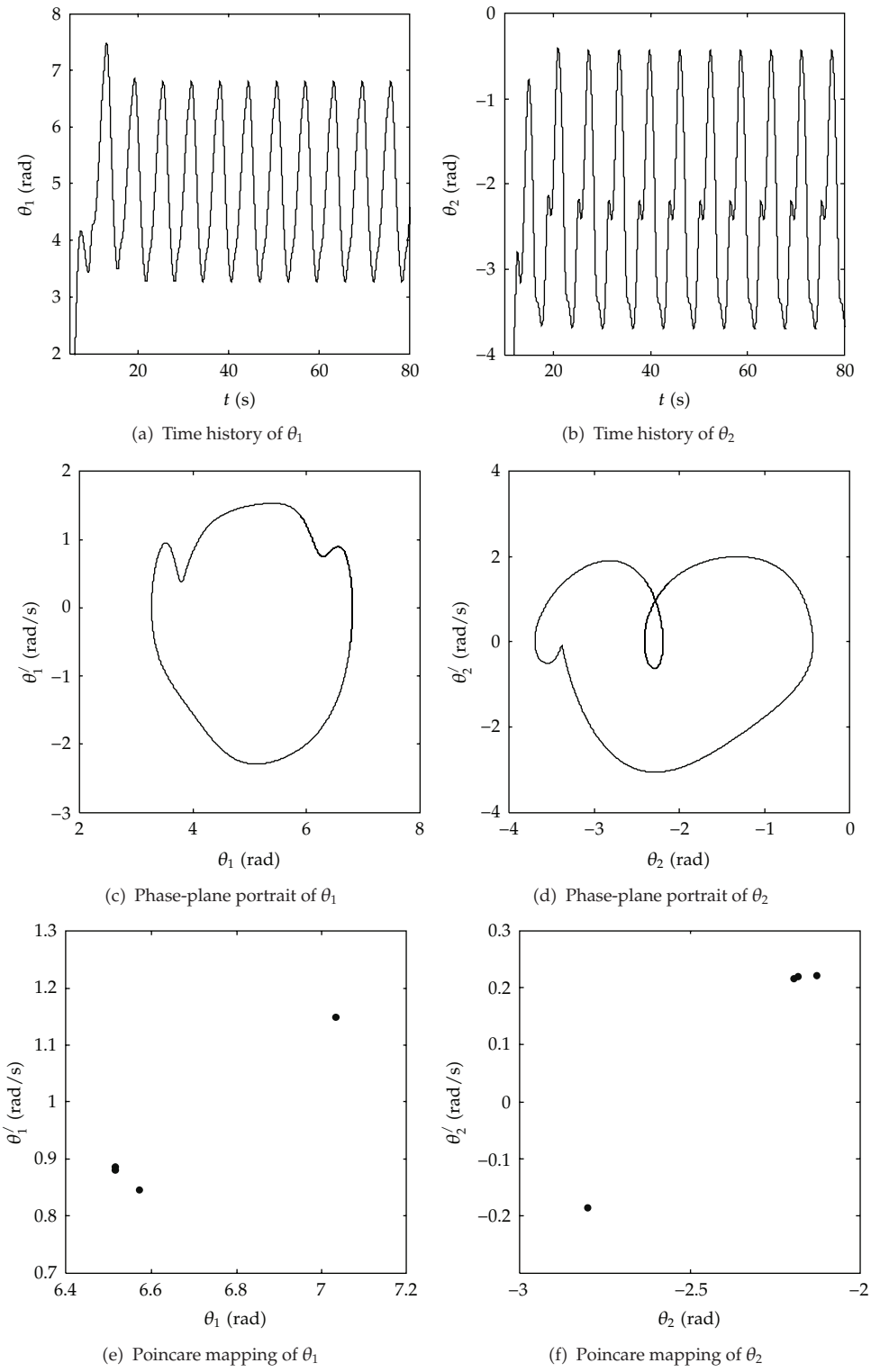

(a) Time history of θ_1

(b) Time history of θ_2

(c) Phase-plane portrait of θ_1

(d) Phase-plane portrait of θ_2

(e) Poincare mapping of θ_1

(f) Poincare mapping of θ_2

Figure 3: Continued.

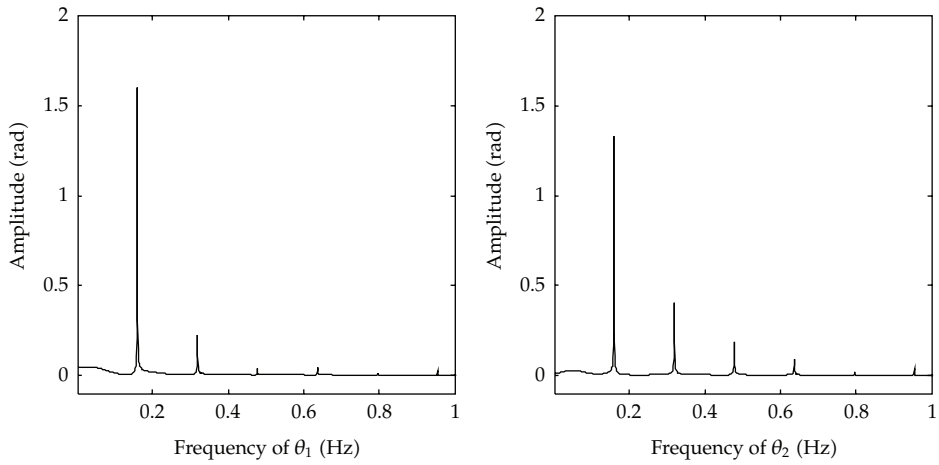

(g) Amplitude spectrum of θ_1 (h) Amplitude spectrum of θ_2

Figure 3: The simulated multiple-periodic motions.

Table 3: The Lyapunov exponents of the simulated chaotic motions of Figure 5.

	First	Second	Third	Fourth	Fifth
θ_1	0.5496	0.0960	−0.0027	−0.1008	−2.0600
θ_2	0.1431	−0.0371	−0.0787	−0.1567	−2.4240

According to the above simulation results, even for the same initial conditions, controlled behaviors vary with the parameters in the controllers. This is because the basins of entrainment, whose counterparts in maps are addressed in [9, 10], depend on the parameters of controller.

4. Discussion on the Simulated Chaotic Motions

In order to quantitatively describe the simulated chaotic motions of the two-bar linkage, Lyapunov exponent and the hypothesis possibility with surrogate data method are used based on nonlinear theory [14–17]. The first five order Lyapunov exponents of the time series of θ_1 and θ_2 are calculated according to algorithm in [14] and shown in Table 3. The calculated hypothesis possibilities with the surrogate data method [17] for the time series of θ_1 and θ_2 are shown in Table 4.

As shown in Table 3, the maximum Lyapunov exponents of the motions of angle θ_1 and θ_2 are 0.5496 and 0.1431, respectively. The positive values indicate that the motions of the two angles are chaotic.

From the calculated hypothesis possibilities with the surrogate data method for the motions of θ_1 and θ_2, that is, 6.3252×10^{-6} and 3.8644×10^{-19}, it is demonstrated that both of them are chaotic due to the checking possibility values which are smaller than .05, referring to an empirical value in [17].

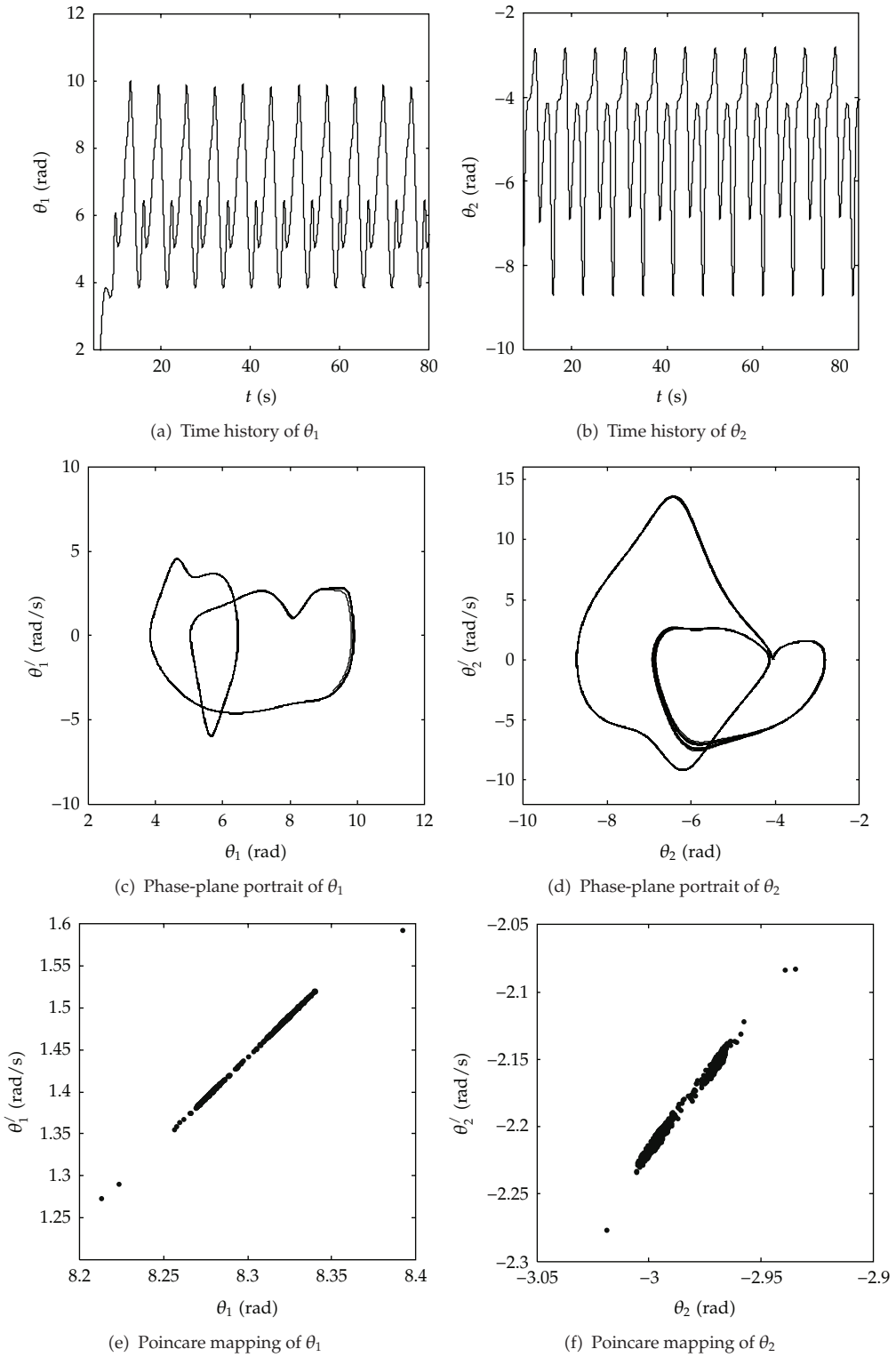

(a) Time history of θ_1

(b) Time history of θ_2

(c) Phase-plane portrait of θ_1

(d) Phase-plane portrait of θ_2

(e) Poincare mapping of θ_1

(f) Poincare mapping of θ_2

Figure 4: Continued.

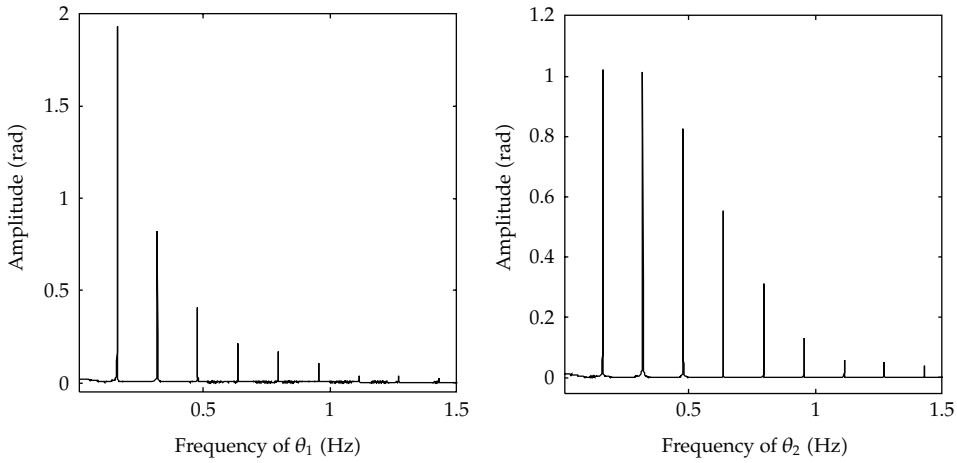

(g) Amplitude spectrum of θ_1 (h) Amplitude spectrum of θ_2

Figure 4: The simulated quasiperiodic motion.

Table 4: The calculated values with surrogate data method for chaotic motions.

	Q_D	μ_s	χ	P
θ_1	5.5241	1.5851	4.5152	6.3252×10^{-6}
θ_2	8.9715	1.5561	8.9408	3.8644×10^{-19}

5. Conclusions

In this paper, the dynamical model of a two-bar linkage with OPCL controller is proposed in order to obtain different motions. It is verified that the OPCL controlled system is asymptotically stable based on the Lyapunov theory, when the control coefficient matrices of **A** and **B** are diagonal and with negative real parts of eigenvalues. It is reliable to force a two-bar linkage to achieve different stable motions of θ_1 and θ_2.

Numeral simulations are conducted to demonstrate that the two-bar linkage can achieve single-periodic, multiple-periodic, quasiperiodic, and chaotic motions by changing the control parameters of **A** and **B** of the OPCL controller for θ_1 and θ_2 successfully. The proposed OPCL approach works on the given conditions.

Furthermore, for the simulated chaotic motions, the maximum Lyapunov exponents are positive, that is, 0.5496 and 0.1431, respectively. The calculated hypothesis possibilities of them with the surrogate data method for the same chaotic motions are 6.3252×10^{-6} and 3.8644×10^{-19}, smaller than .05.

Acknowledgment

The authors gratefully acknowledge that the work was supported by the Key Project of Science and Technology Research Funds of Chinese Ministry of Education (Grant no. 108037).

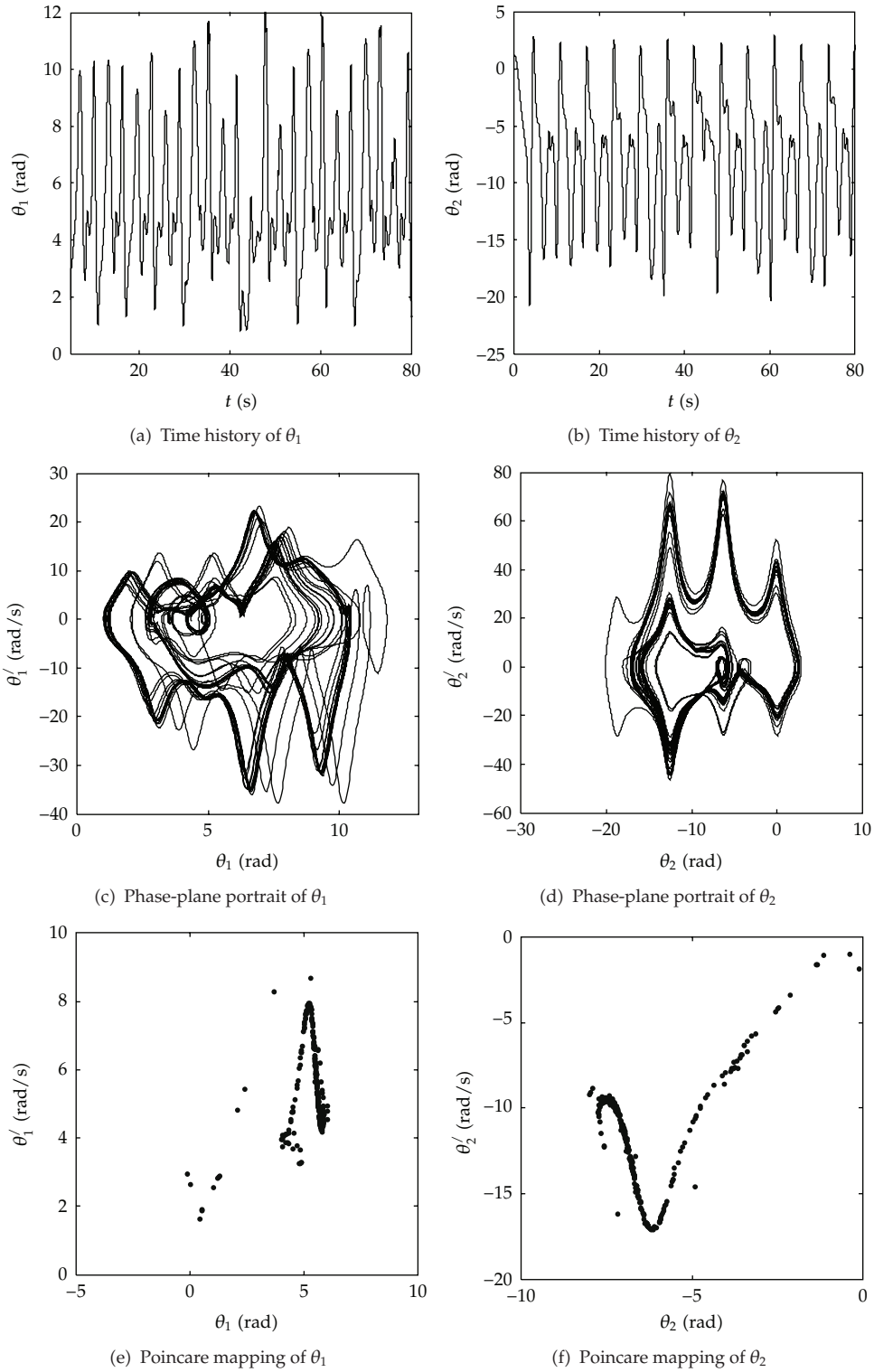

(a) Time history of θ_1

(b) Time history of θ_2

(c) Phase-plane portrait of θ_1

(d) Phase-plane portrait of θ_2

(e) Poincare mapping of θ_1

(f) Poincare mapping of θ_2

Figure 5: Continued.

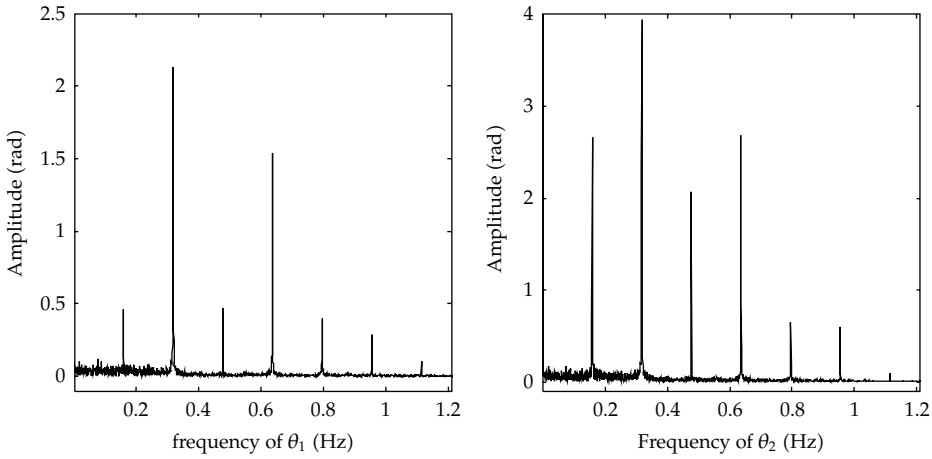

(g) Amplitude spectrum of θ_1 (h) Amplitude spectrum of θ_2

Figure 5: The simulated chaotic motions.

References

[1] K. Matsuoka, N. Ohyama, A. Watanabe, and M. Ooshima, "Control of a giant swing robot using a neural oscillator," in *Proceedings of the 1st International Conference on Natural Computation (ICNC '05)*, vol. 3611 of *Lecture Notes in Computer Science*, pp. 274–282, August 2005.

[2] Q. Han, Z. Qin, X. Yang, and B. Wen, "Rhythmic swing motions of a two-link robot with a neural controller," *International Journal of Innovative Computing, Information and Control*, vol. 3, no. 2, pp. 335–342, 2007.

[3] S. Lankalapalli and A. Ghosal, "Possible chaotic motions in a feedback controlled 2R robot," in *Proceedings of the 13th IEEE International Conference on Robotics and Automation*, pp. 1241–1246, IEEE, April 1996.

[4] A. S. Ravishankar and A. Ghosal, "Nonlinear dynamics and chaotic motions in feedback-controlled two- and three-degree-of-freedom robots," *International Journal of Robotics Research*, vol. 18, no. 1, pp. 93–108, 1999.

[5] F. Verduzco and J. Alvarez, "Bifurcation analysis of A 2-DOF robot manipulator driven by constant torques," *International Journal of Bifurcation and Chaos in Applied Sciences and Engineering*, vol. 9, no. 4, pp. 617–627, 1999.

[6] K. Li, L. Li, and Y. Chen, "Chaotic motion of a planar 2-dof robot," *Machine*, vol. 29, no. 1, pp. 6–8, 2002 (Chinese).

[7] E. A. Jackson and I. Grosu, "An open-plus-closed-loop (OPCL) control of complex dynamic systems," *Physica D*, vol. 85, no. 1-2, pp. 1–9, 1995.

[8] L.-Q. Chen and Y.-Z. Liu, "A modified open-plus-closed-loop approach to control chaos in nonlinear oscillations," *Physics Letters A*, vol. 245, no. 1-2, pp. 87–90, 1998.

[9] L.-Q. Chen, "An open-plus-closed-loop control for discrete chaos and hyperchaos," *Physics Letters A*, vol. 281, no. 5-6, pp. 327–333, 2001.

[10] L.-Q. Chen and Y.-Z. Liu, "An open-plus-closed-loop approach to synchronization of chaotic and hyperchaotic maps," *International Journal of Bifurcation and Chaos*, vol. 12, no. 5, pp. 1219–1225, 2002.

[11] Q.-K. Han, X.-Y. Zhao, and B.-C. Wen, "Synchronization motions of a two-link mechanism with an improved OPCL method," *Applied Mathematics and Mechanics*, vol. 29, no. 12, pp. 1561–1568, 2008.

[12] L.-Q. Chen, "The parametric open-plus-closed-loop control of chaotic maps and its robustness," *Chaos, Solitons and Fractals*, vol. 21, no. 1, pp. 113–118, 2004.

[13] Y.-C. Tian, M. O. Tadé, and J. Tang, "Nonlinear open-plus-closed-loop (NOPCL) control of dynamic systems," *Chaos, solitons and fractals*, vol. 11, no. 7, pp. 1029–1035, 2000.

[14] A. Wolf, J. B. Swift, H. L. Swinney, and J. A. Vastano, "Determining Lyapunov exponents from a time series," *Physica D*, vol. 16, no. 3, pp. 285–317, 1985.

[15] A. A. Tsonis and J. B. Elsner, "Nonlinear prediction as a way of distinguishing chaos from random fractal sequences," *Nature*, vol. 358, no. 6383, pp. 217–220, 1992.
[16] M. T. Rosenstein, J. J. Collins, and C. J. De Luca, "A practical method for calculating largest Lyapunov exponents from small data sets," *Physica D*, vol. 65, no. 1-2, pp. 117–134, 1993.
[17] J. Theiler, S. Eubank, A. Longtin, B. Galdrikian, and J. Doyne Farmer, "Testing for nonlinearity in time series: the method of surrogate data," *Physica D*, vol. 58, no. 1–4, pp. 77–94, 1992.